3D bioprinted alginate-gelatin hydrogel patches containing cardiac spheroids recover heart function in a mouse model of myocardial infarction

Christopher D. Roche [a,b,c], Haiyan Lin [c], Yizhou Huang [b,d,e], Charles E. de Bock [d,e], Dominik Beck [b], Meilang Xue [c], Carmine Gentile [a,b,*]

[a] Faculty of Medicine and Health, University of Sydney, Sydney, NSW, Australia
[b] Faculty of Engineering and IT, University of Technology Sydney (UTS), Sydney, NSW, Australia
[c] Sutton Arthritis Research Laboratory, Kolling Institute, University of Sydney, Sydney, NSW, Australia
[d] Children's Cancer Institute, Lowy Cancer Research Centre, UNSW Sydney, Sydney, NSW, 2052, Australia
[e] School of Women's and Children's Health, UNSW Sydney, Sydney, NSW, 2052, Australia

ARTICLE INFO

ABSTRACT

Epicardial transplantation of 3D bioprinted patches represents a promising protective strategy against infarction-induced myocardial damage. We previously showed that 3D bioprinted tissues containing cardiac spheroids [in alginate/gelatin (AlgGel) hydrogels] promoted cell viability/function and endothelial cell tubular self-assembly. Here, we hypothesise that bioprinted cardiac spheroid patches improve cardiac function after myocardial infarction (MI). To determine treatment effects of hydrogel alone or with cells, MI mice were transplanted with: (i) AlgGel acellular patches, (ii) AlgGel with freely suspended cardiac cells, (iii) AlgGel with cardiac spheroids. We included control MI mice (no treatment) and mice undergoing sham surgery. We performed measurements to 28 days including echocardiography, flow cytometry and transcriptomic analyses. Our results measured median baseline (pre-surgery) left ventricular ejection fraction (LVEF%) for all mice at 66%. Post-surgery, LVEF% was 58% for Sham (non-infarcted) and 41% for MI (no treatment) mice. Patch transplantation increased LVEF%: 55% (acellular; p = 0.012), 59% (cells; p = 0.106), 64% (spheroids; p = 0.010). Flow cytometry demonstrated host cardiac tissue immune cell population changes with treatments. RNAseq transcriptomes demonstrated similar gene expression profiles for Sham and mice treated with cardiac spheroid patches. Extrusion 3D bioprinting permits hydrogel patch generation even preserving microtissue cardiac spheroids directly suspended in the bioink. Inflammatory and genetic mechanisms may play important roles in regulating host responses after patch transplantation in infarcted hearts. Future studies are needed to elucidate the possible immune cell and gene expression-related molecular mechanisms underlying these initial findings.

1. Introduction

Recent advances in 3D bioprinting and cell culture allow fabrication of patches for epicardial transplantation to protect the myocardium [1, 2]. For end-stage heart failure patients there is currently no ideal way to repair damaged heart muscle so that function can be regained, with the gold standard treatment being whole heart allotransplantation [3]. This requires a donor heart to arise (during which time patients may die whilst on a waiting list), major surgery with a significant mortality rate and the need for immunosuppressive drugs for life to reduce the risk of transplant rejection which carry risks of tumour development [4,5]. This unmet need has driven extensive research into many treatment approaches to restore myocardial function [6], of which one promising approach is 3D bioprinting of heart tissue patches for epicardial transplantation [7].

Whilst this field is progressing to human trials, there remain persistent questions about the mechanism by which 3D bioprinted epicardial patches benefit cardiac structure and function after myocardial infarction (MI) [8–13]. Recent evidence suggests host inflammation modulation may be a primary mechanism and not, for instance, pursuit of cell number replenishment [14]. Despite recent advances in this field, additional preclinical studies are required to elucidate optimal conditions for heart patch bioengineering [7,15].

Our laboratory has previously combined 3D bioprinting with

microtissues called "vascularised cardiac spheroids" (VCS) containing cell types found in the human heart [7]. Using extrusion 3D bioprinting systems, these were employed as building blocks for the generation of vascularised viable and functional heart tissues [16]. Given their unique features to recapitulate some of the human heart microenvironment, we hypothesise that 3D bioprinted patches containing VCS can improve cardiac function in mice with MI.

Herein, we present novel results from epicardial transplantation of 3D bioprinted hydrogel-based patches in a surgical MI mouse model following permanent left anterior descending (LAD) artery ligation [15]. We 3D bioprinted patches with alginate/gelatin (AlgGel) and human cardiac fibroblasts (CFs), human coronary artery endothelial cells (HCAECs) and induced pluripotent stem cell-derived cardiomyocytes (iCMs). We examined for differences in cardiac functional and structural outcomes in MI mice receiving patches containing: 1) AlgGel hydrogel alone (MI + PATCH), 2) AlgGel with cardiac cells suspended freely (MI + PATCH CELLS), and 3) AlgGel with VCSs (MI + PATCH SPHEROIDS). Control mice received either a sham procedure (Sham) or LAD ligation without receiving any patch (MI). Finally, flow cytometry, histological and RNAseq analyses of tissues were performed to identify structural, cellular and molecular changes in the different treatment groups.

2. Material and methods

The method was publicly preregistered before the start of the experiment (https://doi.org/10.17605/OSF.IO/7BQEW). The Vevo LAB echocardiography manual (including equations used for echocardiographic parameter calculations) is available from this article's permanent data repository (https://doi.org/10.5281/zenodo.6198612).

2.1. Culture of human cardiac cells

HCAECs (Sigma-Aldrich, MO, United States) were cultured in MesoEndo Growth Medium (Cell Applications, San Diego, CA, United States). CFs (Cell Applications, San Diego, CA, United States) were cultured in Cardiac Fibroblast Growth Medium (Sigma-Aldrich, St Louis, MO, United States). HCAECS and CFs were used for bioprinting at passage three. iCMs (iCell®, FujiFilm Cellular Dynamics, Madison, WI, United States) were cultured according to manufacturer's recommendations in iCell® Cardiomyocytes Maintenance Medium (FujiFilm Cellular Dynamics). In total, ~850,000 cells per $10 \times 10 \times 0.4$ mm patch were used (iCMs: HCAECs: CFs, ratio 1 : 1.5: 2.5).

2.2. VCS formation from cardiac cells

Mixed cardiac cells (iCMs: HCAECs: CFs, in the same ratio 1 : 1.5: 2.5) were suspended in Spheroid Medium (2 : 1: 1 of the iCell Maintenance Medium, MesoEndo and Cardiac Fibroblast Growth Media, respectively). VCSs were generated by coculturing ~10,000 mixed cardiac cells in 15 µl hanging drop cultures in Spheroid Medium, using Perfecta 3D® 384-well hanging drop plates (3D Biomatrix, Ann Arbor, MI, United States). VCSs were allowed to form for up to five days in hanging drops in a humidified incubator at 37 °C with 21% (v/v) O_2 and 5% (v/v) CO_2 following our previous protocol [17]. In total, ~850,000 cells (83 spheroids) per patch were used.

2.3. Hydrogel preparation

Hydrogel was prepared according to our previous method optimised for cardiac applications [7]. Briefly, AlgGel powder – 4 mg alginate and 8 mg gelatin – was sterilised under UV light for 30 min then solubilised at 50 °C in 100 ml Dulbecco's Modified Eagle Medium (DMEM) + 1% (v/v) pen/strep + 1% (v/v) L-glut.

2.4. Bioink generation

To create bioinks for bioprinting, AlgGel was added to pellets of mixed cardiac cells (iCMs, CFs, HCAECs), either as free cells (not in spheroids) or as VCS. Prewarmed (37 °C) AlgGel was added to the cell or VCS pellet by pipette, of which 0.5 ml typically produced six 10 mm^2 patches. The AlgGel was resuspended until the cell pellet disappeared to ensure incorporation of most of the cells. All procedures were performed under a biological safety cabinet and within the bioprinter chamber.

2.5. Heart patch 3D bioprinting

Bioprinting was performed with a BIO X pneumatically driven extrusion 3D bioprinter (CELLINK Life Sciences, Boston, MA, USA). We used an optimised protocol based on our previous method for 3D bioprinting of AlgGel-based patches [7]. Briefly, a 3 ml BIO X syringe was filled with 70% (v/v) ethanol and a CELLINK 25-gauge conical polypropylene nozzle (250 µm inner diameter) attached. The syringe and nozzle were placed in 70% (v/v) ethanol and the bioprinter sterilised with its built-in UV lights. The syringe was then loaded into the bioprinter and an "empty run" was performed to pneumatically cleanse the syringe and nozzle of ethanol by expelling it using high air flow until completely dry (accepting a theoretical risk of some impact on cell viability for the apparent benefit of a contamination rate of zero in our experiments). The printer components were set to 25 °C for the bed and 39 °C for the pneumatic syringe chamber. For ease of transfer of hydrogel to syringe, the pneumatic bung between the pneumatic mechanism and the hydrogel was not used (pneumatic force was transmitted directly through air in the syringe to the hydrogel pool at the lowest part of the syringe and in the nozzle). Adjustments to flow rate and nozzle travel speed were made during the print runs to create optimal patches based on real-time moment-to-moment operator judgement. Patch size was set at $10 \times 10 \times 0.6$ mm with three 0.2 mm layers in the z axis. The grid infill/solidity percentage for the patches was set at 25%. AlgGel was ionically crosslinked on an ice block by adding 4 mls of $CaCl_2$ (2% w/v in PBS) after bioprinting of all the patches in one six-well plate. Then, we cultured patches up to the moment of transplantation (after one and before three weeks of time in culture) based on our previous study determining the optimum moment for transplant [7]. Patches were incubated *in vitro* (one patch in 2 ml Spheroid Medium per well of six-well plates) at 37 °C with 21% (v/v) O_2 and 5% (v/v) CO_2. Our previous patch durability study found movement disturbance of patches was associated with early patch fragmentation [7]. Therefore, movement was minimised (immediate-proximity dedicated incubator, careful low-volume media changes twice a week without disturbance in between). Under these conditions all patches were cultured intact, either until transplantation or *in vitro* analysis.

2.6. In vitro heart patch analyses (confocal microscopy, 3D rendering and multiple electrode array)

Some non-transplanted patches were kept *in vitro* for analysis after 28 days. These patches were stained for nuclei, cardiomyocytes, fibroblasts and endothelial cells (Hoechst stain and antibodies against cTNT, vimentin and CD31/PECAM, respectively) as previously described [18]. Patches were imaged with a Leica Stellaris confocal microscope (Leica Microsystems, Wetzlar, Germany) and 3D rendering analyses were generated using IMARIS visualisation software (Oxford Instruments, Abingdon, Oxfordshire, UK). Some patches were placed on a multiple electrode array (MEA) platform (Mappinglab, Oxford, UK) to confirm the presence of electrical activity.

2.7. Murine MI with heart patch transplantation

We transplanted patches to the epicardial surface of mouse hearts using an optimised protocol based on our previous surgical method [15].

Briefly, male 9–10 week old (mature) B and T cell-depleted B6.Rag1 mice (Australian BioResources, Moss Vale, NSW, Australia) were randomly assigned by an independent facility manager and had their baseline echocardiography. The surgery was performed by one researcher (CG). Anaesthesia was performed by one researcher (CR) with mixed anaesthesia of intraperitoneal ketamine (40 mg/kg) and xylazine (5 mg/kg) plus inhaled isoflurane (5 L/min induction, 0–2 L/min maintenance). Mice were intubated and ventilated then left thoracotomy was performed to gain surgical access to the heart. Mice were assigned to experimental groups by an ethical semi-randomised approach (an ethics-driven approach where randomisation may be altered to reduce the risk of mouse death and where experimental group numbers are added to according to mortality rates with the objective of using the lowest number of mice overall) – in accordance with best ethical practice to reduce mouse numbers in experimental groups for procedures where mortality rates are inherently very high (up to ~50%). The five experimental groups were: 1) Sham surgery (suture passed around the left anterior descending artery (LAD) and tied loosely without occluding the artery); 2) MI by permanent LAD ligation (MI); 3) MI followed by immediate transplantation of a hydrogel (AlgGel) patch without cells (MI + PATCH); 4) MI plus AlgGel patch with freely suspended mixed cardiac (iCM, CF, HCAEC) cells (MI + PATCH CELLS); and 5) MI plus AlgGel patch with mixed cardiac cell VCS (MI + PATCH SPHEROIDS). In the postoperative period, mice were given twice daily subcutaneous buprenorphine injections (0.08 mg/kg) for the first three days after surgery and cared for following standard postoperative protocols for four weeks.

2.8. Cardiac functional analyses (echocardiography)

All mice were imaged using a Vevo 3100 Preclinical Imaging System (FUJIFILM VisualSonics, Toronto, Canada) at baseline, midpoint (day 14) and endpoint (day 28). Echocardiography was performed by one fully trained researcher (CR), with mice under isoflurane anaesthesia via a nose cone (5 L/min induction followed by 2 L/min maintenance). Mice were placed supine on a warming platform and B and M mode echo data were obtained for parasternal long axis and short axis views. Long axis data were analysed using the AutoLV (automatic artificial intelligence-based analysis) function by one researcher (CR) and validity confirmed independently (blind) by a VisualSonics data specialist (FUJIFILM Visualsonics, Toronto, Canada).

2.9. Electrical mapping

Electrical mapping was performed by trained researchers (CR and CG) using an EMS64-USB-1003 Electrical Mapping System and EMap-Record/Scope software (MappingLab, Oxford, UK). Electrical activity mapping data were obtained by placement of a probe onto the epicardial surface or patch in the open chest at surgery. Data were obtained at timepoints: baseline (pre-MI); immediately after LAD ligation (post-MI); immediately after patch transplantation (post-PATCH); and at the end of experiment at day 28 (END). Independent data validation, analyses and processing were performed by a MappingLab data specialist (Yatong Li) and a high inclusion threshold for data quality was used.

2.10. Structural (histological) analyses

At 28 days post procedure, mice were euthanised and 1 mm heart tissue transverse (axial) slices of the left ventricle (distal to the LAD ligation) were obtained for structural analyses (histology, flow cytometry and mRNA analysis).

Histological tissue analyses. Histology (H&E, PicroSirius Red, Masson's Trichrome) was performed on 4 μm transverse heart tissue sections. Slides were digitalised and infarct size calculated by the midline infarct arc length method [19]. Measurement and analyses were performed blind followed by unblinding at the stage of processing data for visualisation. Mice that died before day 28 had post-mortem performed and samples sent for independent (blind) histological analysis (Cerberus Sciences, Melbourne, Australia).

2.11. Cell quantification by flow cytometry

Flow cytometry was performed on heart tissue using a BD LSRFortessa™ flow cytometer and data analysed by BD FACSDiva software (BD Biosciences, Franklin Lakes, NJ, United States) – full list of antibodies used for staining in the Supplementary Materials. Samples were taken and processed immediately based on our previously reported protocol [20]. Briefly, tissue samples were chopped into small pieces and subjected to Liberase™ (Roche Diagnostics, NSW, Australia) digestion. Liberated cells were incubated with a cocktail of primary antibodies for 45 min at room temperature before processing through the cell cytometer. Flow cytometry data were analysed as relative numbers (no comparison of absolute numbers was performed for batches processed on different occasions).

2.12. RNAseq analyses

Cardiac apex samples were processed for mRNA transcriptomic analysis according to the protocol of a commercially available mRNA isolation kit (RNeasy Fibrous Tissue Mini Kit, Qiagen, Cat no. 74704, Hilden, Germany). Total RNA from cardiac apical cells was isolated (phenol– 17 chloroform separation of TRIzol LS) and purified according to the manufacturer's instructions. RNA quality assessment, library preparation, and sequencing were performed by BGI Genomics (Hong Kong, China) using DNBSEQTM sequencing technology and an Agilent 2100 Bioanalyzer (see the Supplementary Materials for full RNA sample data including RNA Integrity Number (RIN) per sample). Samples were independently processed by BGI (Batch no. INSP21000010163). Raw sequencing reads were filtered for adapters – reads in which more than 10% of bases were unknown and reads in which more than 50% of bases were low quality (base quality <20). The resultant high-quality reads were aligned to the mouse genome (mm10) using the software STAR (Spliced Transcripts Alignment to a Reference) [21] with standard parameters. We mapped an average of 26,346,213 reads per sample achieving an average alignment rate was 98.78%. Gene expression levels were quantified using the tool featureCounts [22]. Expression levels were normalized using the software package DeSeq2 [23] in the R statistical analysis software [24]. Genome-wide expression profiles were analysed using principal component analysis (PCA). Hierarchical clustering with average linkage and Euclidean distance was performed using Partek Genomics Suite® (Partek®, St Louis, MO, USA).

2.13. Statistical analyses

Results were analysed using PRISM (GraphPad, San Diego, CA, United States). Stepwise hypothesis testing for continuous data was performed using two-tailed Mann–Whitney U tests with Bonferroni correction or Kruskal-Wallis tests (for a difference in more than two groups). Hypothesis testing of categorical data was performed with two-tailed Fisher's exact contingency testing. Kaplan-Meier survival curve hypothesis testing was performed using the Log-rank (Mantel-Cox) test.

3. Results

3.1. 3D bioprinted VCS patches present stable and functional spheroids at 28 days

Cultured under minimal movement conditions, all patches remained intact for at least 28 days in the incubator. Our analysis of 3D bioprinted patches at 28 days post incubation demonstrated the presence of VCS (stained with antibodies for iCMs (cTNT), CFs (vimentin) and HCAECs (CD31), Fig. 1 and Videos 1, 2 and 3). Our analysis also demonstrated
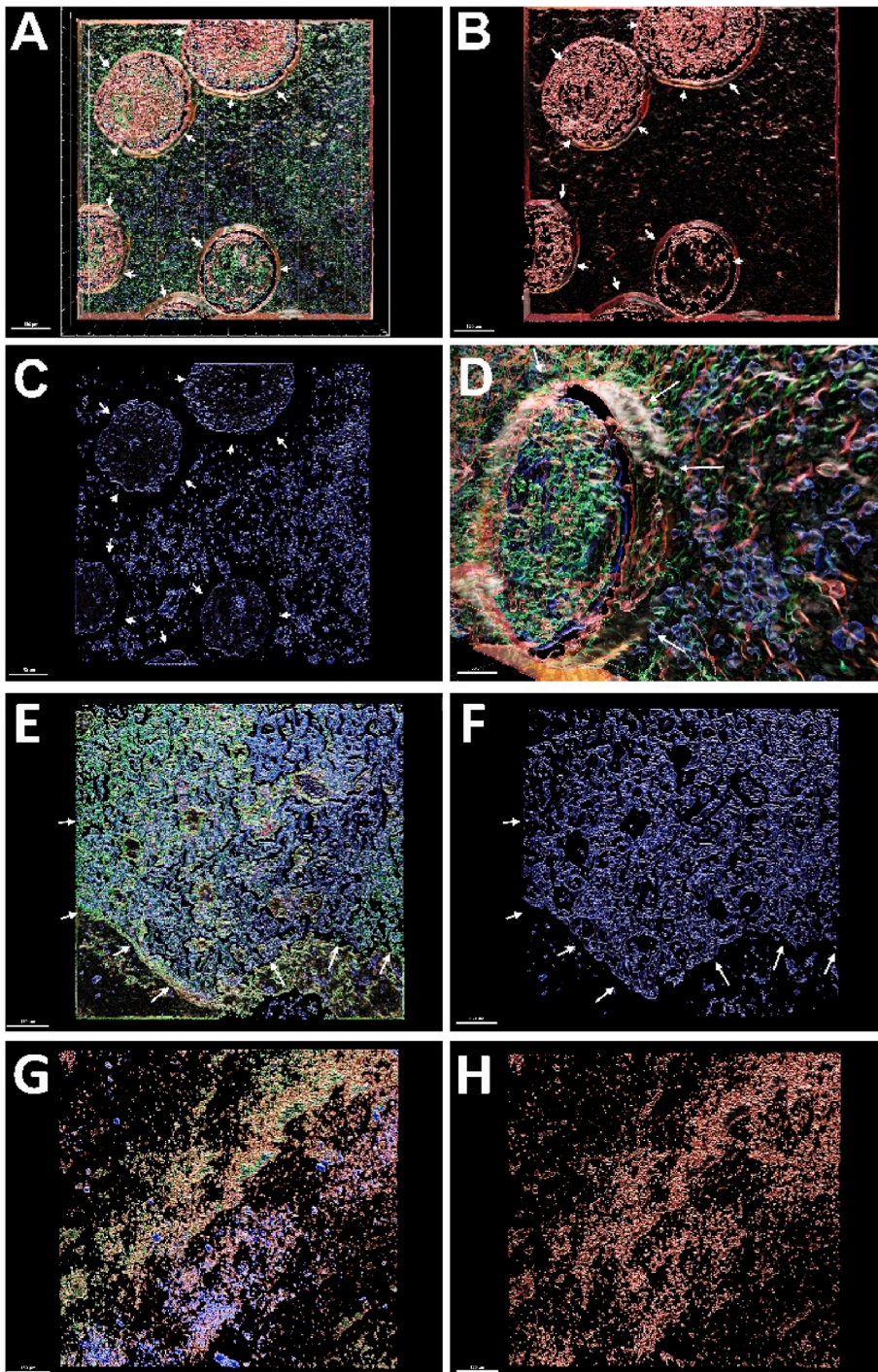
Fig. 1. Cardiac spheroids (A–D) and freely suspended cardiac cells (E–H) with endothelial cell networks present at 28 days in 3D bioprinted patches. (A) Overview of a 3D rendered region of a cardiac spheroid patch stained with antibodies for cardiomyocytes (red, cTNT), endothelial cells (blue, CD31) and fibroblasts (green, vimentin). (A) Shows the overlay, whereas (B) and (C) show the cardiomyocyte and the endothelial cell population, respectively. (D) Is a side closeup view of a spheroid from (A). Arrows point at spheroids within the patch. Fig. 1. (E–H) 3D rendering analyses of bioprinted patches containing cardiac cells (not in spheroid conformation) at 28 days that were stained with antibodies for cardiomyocytes (red, cTNT), endothelial cells (blue, CD31) and fibroblasts (green, vimentin), respectively. Arrows in (A) and (B) indicate the extensive endothelial cell network formed within the patch. (C–D) Single cells are observed in certain areas of the patch in the periphery, indicating absence of complete maturation in these areas. These data are also visualised in 3D-rendered video format for Videos 1, 2 and 3 (full-length videos are in the data repository). Due to the resources required to obtain 3D large-sample multichannel images for cell patches, no imaging of acellular (hydrogel only) patches were taken. Scale bars = 150 μm). (For interpretation of the references to colour in this figure legend, the reader is referred to the Web version of this article.)

that HCAECs self-assembled into networks, both within and outside of spheroids (Fig. 1 and Video 2). Overall, our analyses of cell structures in patches *in vitro* provided evidence that cells within our AlgGel patches formed endothelial cell networks, consistent with our previous reports [7,17]. We detected electrical signals within our patches supporting a degree of electrical activity at 28 days (Suppl. Fig. 1). This is consistent with our previous report of cardiomyocyte activity in patches incubated *in vitro* over 28 days [7].

Supplementary video related to this article can be found at https ://doi.org/10.1016/j.bprint.2023.e00263

3.2. Transplantation of patches containing VCS protected against MI-induced reduction in cardiac function

Results for our primary functional outcome (LVEF%) are shown in Fig. 2. The increased LVEF% with treatment was consistent with our secondary analyses of other functional echocardiographic parameters (Suppl. Fig. 2). The increased LVEF% of the MI + PATCH SPHEROID group was consistent with that group's favourable electrical activity profile (Figs. 3 and 5 and Suppl. Fig. 2).

Median baseline (before surgery) LVEF% from all mice (survivors and non-survivors) was 66% (IQR 61–70; n = 51) with a similar mean ± SD (65 ± 8). Baseline characteristics and 28-day mortality rates were
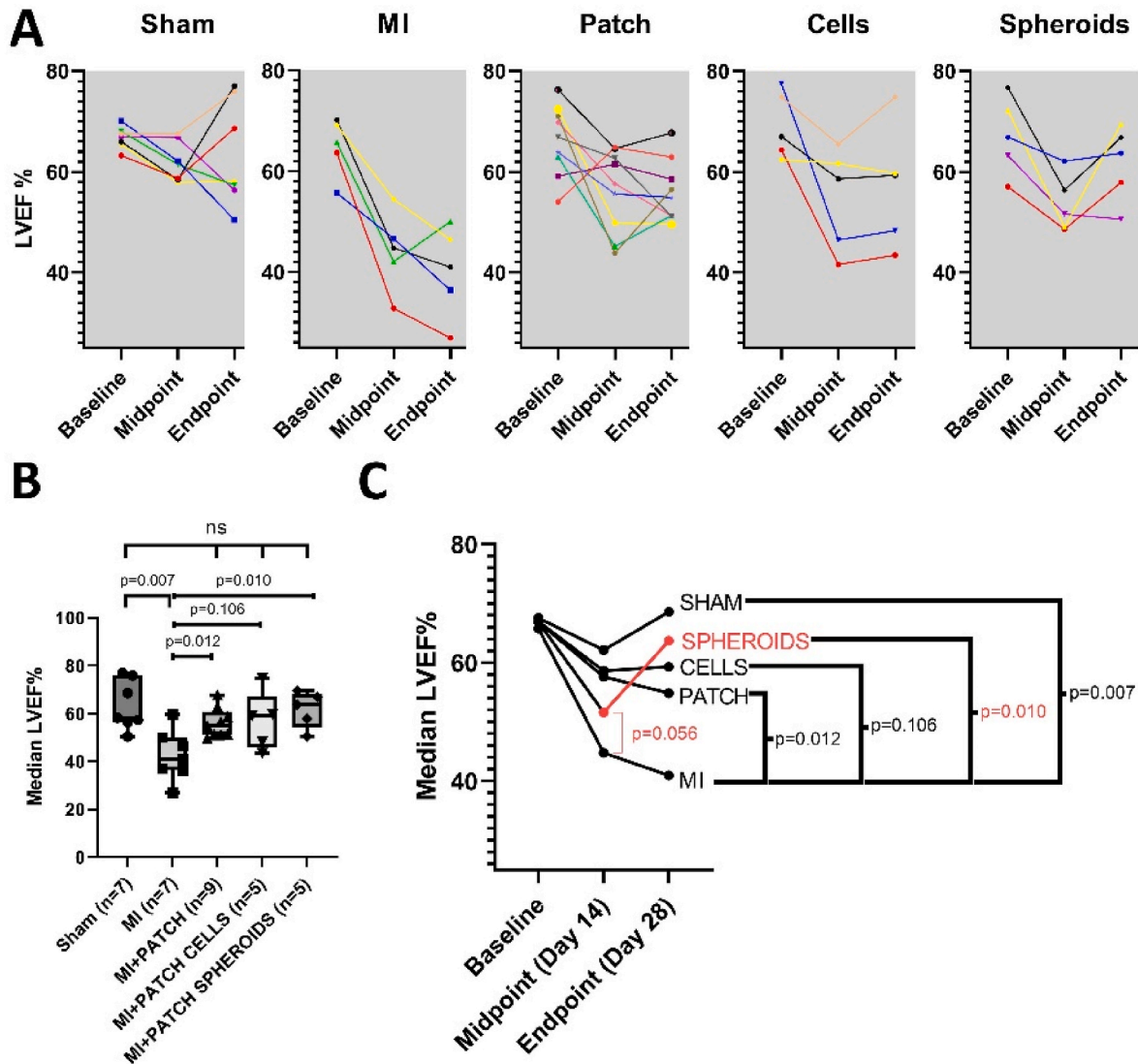
Fig. 2. Patch transplantation protects against MI-induced reduction in cardiac function. (A) Sequential LVEF% values for each experimental group taken at baseline (before surgery), midpoint (14 days after surgery) and endpoint (28 days after surgery). For each group, individual lines on the graph show individual mice. Variability in the LVEF% was observed in individual mice as shown by high variability in endpoint values for sham mice and high variability in baseline values in all groups. Compared to MI, all three treatment groups trended towards higher LVEF% values at both midpoint and endpoint. (B) Median LVEF% for each treatment group at day 28 shows a trend towards increasing improvements in LVEF%. (C) Median LVEF% per group at baseline, midpoint and endpoint; For other functional outcome measures (fractional shortening and cardiac output) see Suppl Fig. 2. Error bars show interquartile range; p values calculated with pairwise Mann-Whitney U tests.

similar between groups with overall mouse survival at 56% (Suppl. Fig. 3).

Patches containing VCS increased the median LVEF% from 41% to 64% compared to control infarcted mice at 28 days (Fig. 2). On pairwise hypothesis testing between groups, LVEF% for the MI group (LAD ligation and no patch) had a statistically significant difference compared to all groups except for MI + PATCH CELLS (Fig. 2). There was no statistically significant difference between treatment groups (MI + PATCH, MI + PATCH CELLS, MI + PATCH SPHEROIDS) or between each treatment group and Sham (Sham day 28 median LVEF% = 58 (IQR 57–72; n = 7)). Overall, the median LVEF% was increased from 41% for MI (IQR 37–48; n = 7) to: 55% (IQR 51–59; n = 7), 59% (IQR 48–60; n = 5) and 64% (IQR 58–67; n = 5) with MI + PATCH, MI + PATCH CELLS or MI + PATCH SPHEROIDS, respectively.

These results show a trend back towards 'baseline' LVEF% values with any of the three patch groups. Whilst MI + PATCH SPHEROIDS presented the largest increase in LVEF% (compared to MI), even patches without cells presented an absolute value increase of 15%. With such an increase in the MI + PATCH control group, the study did not detect a statistically significant difference between patches with spheroids (absolute value increase 23%) and patches with no cells at all.

3.3. Transplantation of VCS-containing patches did not have significant effects on conduction velocity

To evaluate electrical activity modulation, conduction velocity (CV) was analysed using 64-electrode electrical maps (Fig. 3). There was a drop in the mean CV between the Sham and MI group at the time of surgery. No difference was detected between any of the day 28 CVs (p = 0.86 (n = 20); Kruskal-Wallis test) (Fig. 3). Comparison of CVs for immediately post-MI against day 28 was not statistically significant for any group where LAD ligation was performed (respective day 28 medians (mm/ms) were: 0.56 (MI), 0.69 (MI + PATCH), 0.82 (MI + PATCH + CELLS) and 0.56 (MI + PATCH + SPHEROIDS); p = 0.21 (n = 42) Kruskal-Wallis test) (Fig. 3). Overall, LAD ligation (MI) seemed to decrease conduction velocity to 68–75% of its normal value (at the time
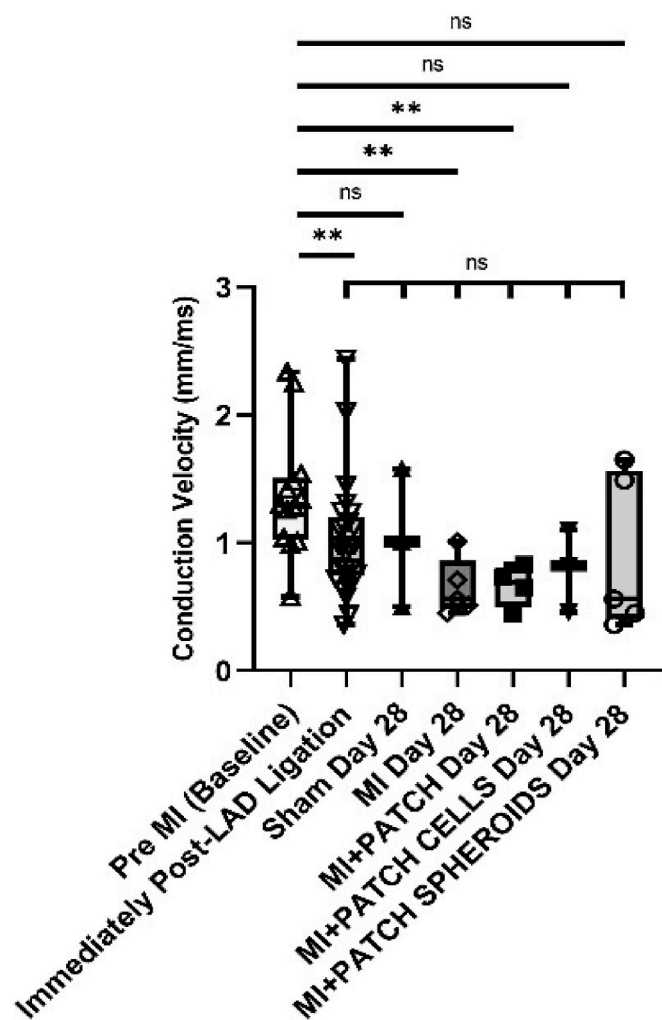
Fig. 3. No treatment rescued mean CV by day 28 following LAD ligation. Left anterior descending artery (LAD) ligation immediately reduced the median conduction velocity (CV) compared to pre-MI (baseline) values (taken immediately before LAD ligation). The statistically significant difference between pre-MI (baseline) values and post LAD ligation values (on day zero) seemed to persist up to day 28 (that is, there was no evidence of a return in CV back towards baseline values detected at this level of statistical power). In fact, the trend in the MI group was for the CV to fall further by day 28 in parallel with falling cardiac function (see also Fig. 2). Overall, reduction in CV was seen with LAD ligation and there was no evidence of recovery by day 28. Error bars show quartile range, p values were calculated using stepwise Mann-Whitney U tests (Bonferroni-corrected level of significance is p = 0.0083 for six stepwise calculations against pre-MI baseline values and p = 0.010 for five stepwise calculations against values taken immediately post-LAD ligation). Only high quality 64 electrode electrical mapping readings were used in this analysis and where there was any question about the quality of individual readings that reading was not used.

it was performed) and this change persisted until day 28.

3.4. Infarct size trended downwards in mice receiving VCS containing patches compared to MI

Transplantation of patches containing cardiac spheroids showed a trend towards smaller infarct sizes (Fig. 4). There was a trend towards decreasing infarct size moving through treatment groups from MI to MI + PATCH, MI + PATCH CELLS and then to MI + PATCH SPHEROIDS (Fig. 4). Reducing infarct size was strongly correlated with increasing LVEF% for the MI group, weakly correlated for the MI + PATCH group and not correlated for the MI + PATCH SPHEROIDS group (R squared

values, 66%, 15% and 0.3%, respectively) (Fig. 4E). Infarct patterns were variable (Fig. 4A–C), with mice showing varying infarct region appearances. Variable infarction pattern was also reported by our independent post-mortem histological analysis of mice that died in the postoperative period (see the Data Repository https://doi.org/10.5281/zenodo.6198612). In 4 out of 5 mice in the MI + PATCH CELLS group, regional infarctions were not detected, consistent with independent post-mortem analysis of mice that died before day 28 (Cerberus Sciences). In that post-mortem analysis, infarctions were observed in focal segments (including regional infarcts only affecting the cardiac apex) and overall infarct size showed a variable range of ~20–70% (see the data repository).

3.5. Integrative analysis of CV and LVEF%

We next sought to investigate potential mechanisms underlying the variability of treatment responses within each group. We analysed coefficients of determination (R squared expressed as a %) for the relationship of CV (electrical mapping) to the LVEF% (Fig. 5). Additionally, we performed representative side-by-side analysis of the electrical map at day one (immediately after LAD ligation), electrical map at day 28, and LVEF% progression (baseline – midpoint – endpoint) for individual mice. Electrical maps on day one (Fig. 5C, F, I, L) were similar to a baseline (pre-LAD ligation) map (Fig. 5A). The MI + PATCH CELLS representative mouse was the only mouse in this analysis which showed no improvement in LVEF% from day 14 (midpoint) to day 28 (endpoint) – the other mice (sham, MI + PATCH and MI + PATCH SPHEROIDS) all showed a V-shaped LVEF% progression, with a drop at midpoint and recovery at endpoint (Fig. 5). Sham group mice (needle and suture passed under the LAD and tied loosely without occlusion) also showed variability in LVEF% (Fig. 5B) despite having no infarction – representing the impact of the cardiac surgical model itself.

### 3.6. Tissue immune cell analysis by flow cytometry

Recent reports suggested that mechanisms regulating myocardial regeneration by using cells/materials in contact with the host heart may be dependent on the innate immune response in the host [14,25,26]. Therefore, we performed host (mouse) tissue immune cell population analyses in heart tissues isolated at day 28 using flow cytometry and quantified the absolute immune cell count for each group (Fig. 6).

For macrophages, we demonstrated a trend towards reversal of the M1:M2 macrophage ratio from 3.4:1 (sham) to 1:4 (MI), accompanied by a partial return towards sham values with each of our three treatment groups (Fig. 6A). Despite the M1:M2 ratio being a dichotomous simplification of a complex continuum [25], our results demonstrate that the addition of the patch can play a role on macrophage activity. The ratio of neutrophils to monocytes favoured a monocyte dominance only for the MI + PATCH SPHEROIDS group (compared to all other groups, including sham) (Fig. 6B). For all groups, there were proportional changes in tissue monocytes and tissue macrophages compared to all other live singlet immune cells (Fig. 6C and D).

For natural killer cells (NKs) there was a reduction in the number of these cells in all treatment groups compared to MI (Fig. 6E). The same analysis demonstrated an increase in the proportion of haematopoietic stem cells (HSCs) within all treatment groups compared to MI and Sham (Fig. 6F). Overall, our results demonstrated changes in host immune cell numbers on day 28, suggesting that host immune system modulation may be an important mechanism underlying the benefits of epicardial patch transplantation for MI.

3.7. The transcriptomic profile for the spheroid group was similar to sham (non infarcted)

Whole mouse transcriptomes were profiled in triplicates for samples from five groups MI, MI + PATCH, MI + PATCH CELLS, MI + PATCH
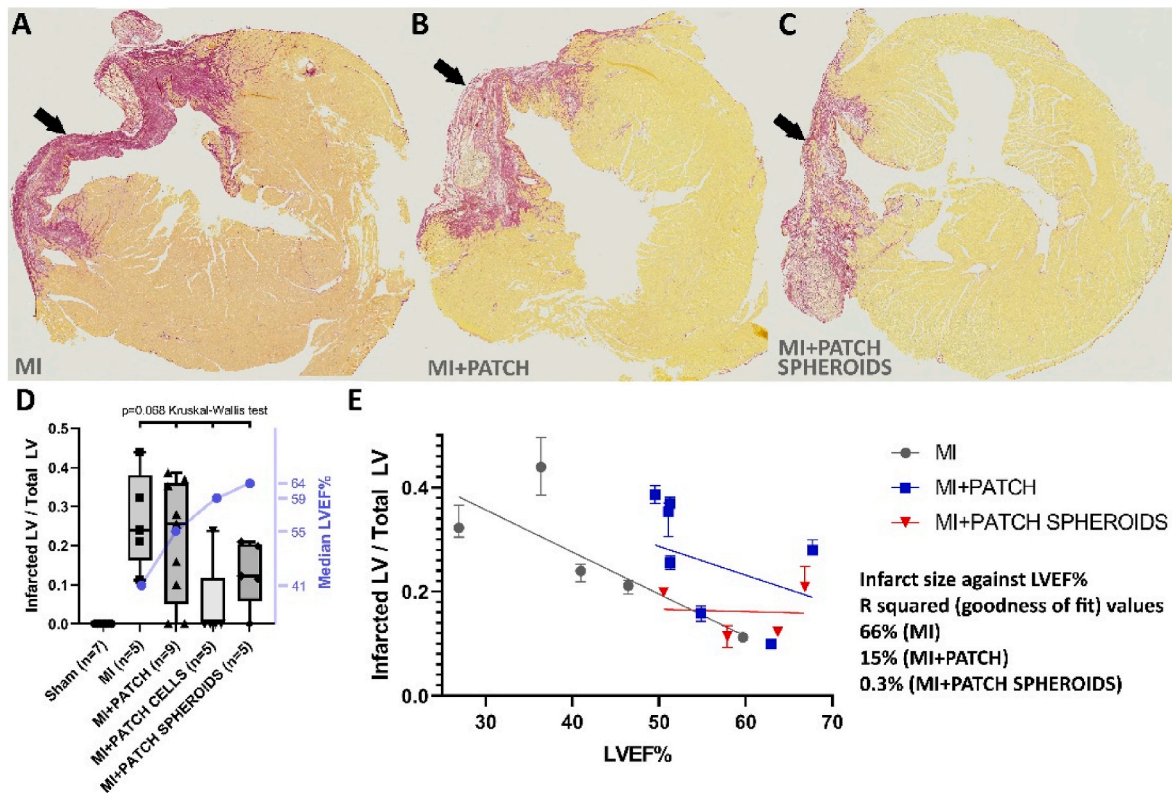
Fig. 4. In mice surviving up to 28 days, the strong correlation between infarct size and LVEF% in the MI group was reduced for the MI + PATCH group and reduced further for the MI + PATCH SPHEROIDS group. (A–C) Infarction (collagen) staining with Picrosirius Red (PSR) for a mouse in the MI group (A), MI + PATCH group (B) and MI + PATCH SPHEROIDS group (C) shows that infarct patterns were variable (black arrows point to infarcted area stained with PSR). (D) Shows infarct size (infarcted LV/Total LV) across groups. Median LVEF% for each group is plotted as a blue line (values on the right Y axis). There was a trend towards a lower infarct size between the MI group and the interventional groups (MI + PATCH, MI + PATCH CELLS, MI + PATCH SPHEROIDS) but the result was not statistically significant. (E) Shows coefficients of determination (R squared) values for the LVEF% plotted against the infarct area (sham not shown as no LAD ligation was performed and infarct size was zero in all cases). The moderately strong correlation between LVEF% and infarct size in the MI group (66%) was disrupted in treatment groups MI + PATCH (15%) or MI + PATCH SPHEROIDS (0.3%). This may suggest a protective effect beyond reduction of circumferential infarct size (decoupling the direct relationship of higher infarct size with lower LVEF% seen for MI without treatment and suggesting that the density of the infarction observed in (A) may be reduced (C) and function (D) protected). Points on graph represent individual mice (median infarct size from multiple repeat measurements of different histological sections; error bars show IQR) and goodness of fit (R squared) to trend lines is expressed as a percentage. Only mice with infarct size >0 were used for this analysis. (For interpretation of the references to colour in this figure legend, the reader is referred to the Web version of this article.)

SPHEROIDS, and Sham. PCA of mouse transcriptomes identified samples segregating into three visual clusters including cluster 1 with samples from MI as well as MI + PATCH ("Patch"), cluster 2 with samples from MI + PATCH CELLS ("Cells"), and cluster 3 with samples from MI + PATCH SPHEROIDS ("Spheroids") as well as Sham (Fig. 7A). Cluster 3 also contained an outlier from the group of "Cells" (sample number 50). Differential gene expression analysis comparing all sample groups identified 462 transcripts that were significantly different between groups (p-value 0.05 and fc > |1.5|; Supplementary Tables S1–10). Hierarchical clustering of these transcripts confirmed the clustering previously observed by principal component analysis (Fig. 7B). We found that there were no differentially expressed transcripts when samples of the Sham and Spheroids groups were compared, suggesting that these cells were indeed molecularly similar.

To determine the molecular responses of MI cells treated with VCS, we further interrogated the expression of 97 transcripts differentially expressed between samples in these two groups (Supplementary Table S3). Hierarchical cluster analysis of these transcripts showed that exposure of MI cells to Spheroids led to dominant molecular repression of gene expression (Figs. 7C and 79 genes down and 18 genes up). The same gene expression program was also recapitulated in samples from Sham (that is, the spheroid-treated group and the non-infarcted sham group were molecularly similar).
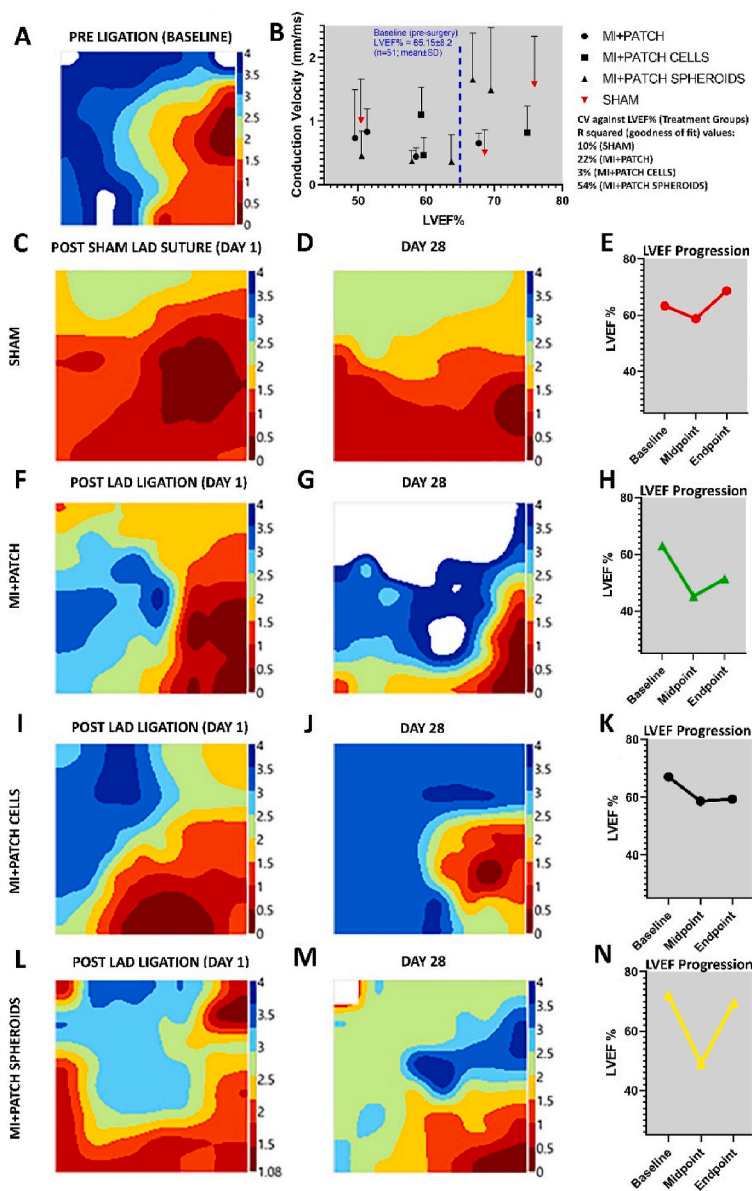
When interrogated for biological pathways, we found that these

genes showed a clear enrichment for functions associated with Cardiovascular System Development and Function as well as Cellular Development, Growth, Proliferation, Assembly and Organization (Fig. 7D, top panel, Supplementary Table S11).

Within the subset of pathways associated with Cardiovascular System Development and Function the repression of the genes ASPH, ATP2A2, KCNJ11, MYL4, MYL7, RYR2 and CLU were strongly associated with the regulation of contraction of the heart, cardiac contractility, and contraction of cardiac muscles (Fig. 7D, bottom panel, Supplementary Table S12). Enrichment analysis for canonical pathways highlighted relevant pathways associated with beta adrenergic signalling and dilated cardiomyopathy (Supplementary Figs. 4–6).

4. Discussion

Our study adds to the evidence that 3D bioprinted epicardial patches protect the myocardium after MI. Moreover, our "return-to-baseline" cardiac functional results (Fig. 2) are promising. Our initial analyses raise an interesting mechanistic proposition: that stimulating host immune cells (Fig. 6) by subjecting them to contact with foreign material could account for some (but not all) of the cardiac functional benefit we observed. The rest of the benefit may be influenced by gene expression changes (Fig. 7). This might explain why only our most successful (spheroid) treatment group "reversed" the transcriptomic profile for MI

A PRE LIGATION (BASELINE)

B

Baseline (pre-surgery) LVEF% = 65.15±8.2 (n=51; mean±SD)

Conduction Velocity (mm/ms)

LVEF%

● MI+PATCH
■ MI+PATCH CELLS
▲ MI+PATCH SPHEROIDS
▼ SHAM

CV against LVEF% (Treatment Groups)
R squared (goodness of fit) values:
10% (SHAM)
22% (MI+PATCH)
3% (MI+PATCH CELLS)
54% (MI+PATCH SPHEROIDS)

C POST SHAM LAD SUTURE (DAY 1)   SHAM

D DAY 28

E LVEF Progression — LVEF % — Baseline, Midpoint, Endpoint

F POST LAD LIGATION (DAY 1)   MI+PATCH

G DAY 28

H LVEF Progression — LVEF % — Baseline, Midpoint, Endpoint

I POST LAD LIGATION (DAY 1)   MI+PATCH CELLS

J DAY 28

K LVEF Progression — LVEF % — Baseline, Midpoint, Endpoint

L POST LAD LIGATION (DAY 1)   MI+PATCH SPHEROIDS

M DAY 28

N LVEF Progression — LVEF % — Baseline, Midpoint, Endpoint

Fig. 5. Electrical remodelling of the infarcted LV may be an important mechanism contributing to improved LVEF%. (A) Representative image of a baseline (pre-MI) 64-electrode array electrical map (isochronal activation map) of the anterior cardiac surface. The isochronal (AT) map represents the sequential event of depolarisation. It is constructed with relative values to the earliest activation time from 64 channels. The deep red colour means the earliest activation site. More red colours on a map means fast CVs. AT map from post LAD ligation readings (C, F, I, L) show that the normal pathway for conductive activation is mainly blocked (red meets blue, the loss of colour gradient) in the MI area (in blue). This gradient (seen in the baseline (pre-ligation) map in A) is not fully recovered after all of treatments (G, J, M) possibly due to the formation of scar tissues. (B) Day 28 mean LVEF% (n = 1 repeat reading per mouse from best echocardiographic trace of up to 7 sequentially acquired traces) plotted against mean CV (n = 4 repeat readings per mouse) (error bars = SD; only upper bar shown). Sham group values show wide variation in LVEF% on day 28 even with only a sham procedure (see also Fig. 2A). Wide error bars show variability in CV readings. The MI + PATCH SPHEROID group seemed to trend towards increasing overall mean CV with increasing LVEF%. (C–E) For a mouse underdoing a sham procedure AT maps on day one at surgery (C) and day 28 (D) were similar. (E) Shows the corresponding baseline (day one before surgery), midpoint (day 14 after surgery) and endpoint (day 28) LVEF% for the same sham group mouse. (F–H) For a mouse undergoing MI + PATCH transplantation electrical maps on day one post-LAD ligation (F) and day 28 (G) show loss of colour gradient and a white area where no signal was detected. (I–K) Electrical maps for this MI + PATCH CELLS mouse (with a cellular patch transplanted) shows partial recovery of the electrical map. The day 28 electrical map (J) showed a greater area of blue squares (slow CV) and more abrupt transition between fast (red) and slow (blue) areas when compared to day one for that mouse (I). The corresponding LVEF% (K) was similar compared to other groups with a decrease at the midpoint and partial recovery by the endpoint. (L–N) For a mouse in the MI + PATCH SPHEROIDS group, electrical maps (L–M) showed partial recovery of gradient. The corresponding LVEF% showed a steep uptick between midpoint and endpoint (N). (For interpretation of the references to colour in this figure legend, the reader is referred to the Web version of this article.)

mice (to resemble non-infarcted (sham) mice by day 28).

For this study we focused on *in vivo* outcomes since we had performed *in vitro* analyses of different 3D bioprinters and bioinks in our previous studies [7,17]. Patch disturbance reduction thanks to limited handling of patches based on our previous research [7] helped in performing our *in vitro* analyses (Fig. 1 and Supplementary Fig. 1).

For cardiac functional outcomes *in vivo*, our results suggest that a clinically significant rise in LVEF% (absolute value gain of ~20%) can be achieved by patch transplantation in mice modelling acute MI. This adds further evidence to other reports that this treatment strategy is effective [6,27–29]. The full mechanism remains unknown but our results do not refute the proposition that the mechanism may be associated with stimulating a host innate immune system response; suggested by Vagnozzi et al. (2019) with a myocardial injection-ischaemia/reperfusion injury model [14]. Our findings (especially that hydrogel with no cells has some effect) are consistent with human trials reporting potential improvements in function even with a limited cell density in patches transplanted to the epicardium [12]. In our study, we report that even without cells, hydrogel alone transplanted to the epicardium (in the acute phase of MI) raised the LVEF% from 41% to 55% (Fig. 2). Some might interpret this to mean that all our treatment groups (cells or not) reversed a heart failure state to an acceptable (non-heart failure) state. Interpreted in this way, our results may not support the hypothesis that cell spheroids offer a clinically significant advantage over our other treatments. Similarly, the small (statistically non-significant) potential difference between our spheroid group (~64% median LVEF%) and freely suspended cells group (~59%) would represent only an absolute increase of ~5% on top of the ~20% observed compared to MI without treatment (~41%).

Nonetheless, we showed a trend towards incremental increases in LVEF% with the addition of cells and then cell spheroids compared to AlgGel patches without cells (Fig. 2). Mechanistically, if underlying host immune-genetic modulation is important (Figs. 6 and 7), this raises an interesting consideration. Specifically, it calls into question whether cell number replenishment strategies – or even the goals of host-patch vascular network anastomoses (Fig. 1 and Video 3) and electrical activity integration (Figs. 3 and 5 and Suppl. Fig. 1) – would be fully aligned with the underlying mechanistic processes conferring myocardial protection. To proceed with human trials [8,10,12] without understanding mechanisms may subject patients to treatments which are not aligned with the underlying reason why they work [30]. Better understanding of the mechanisms regulating optimal prognosis in heart
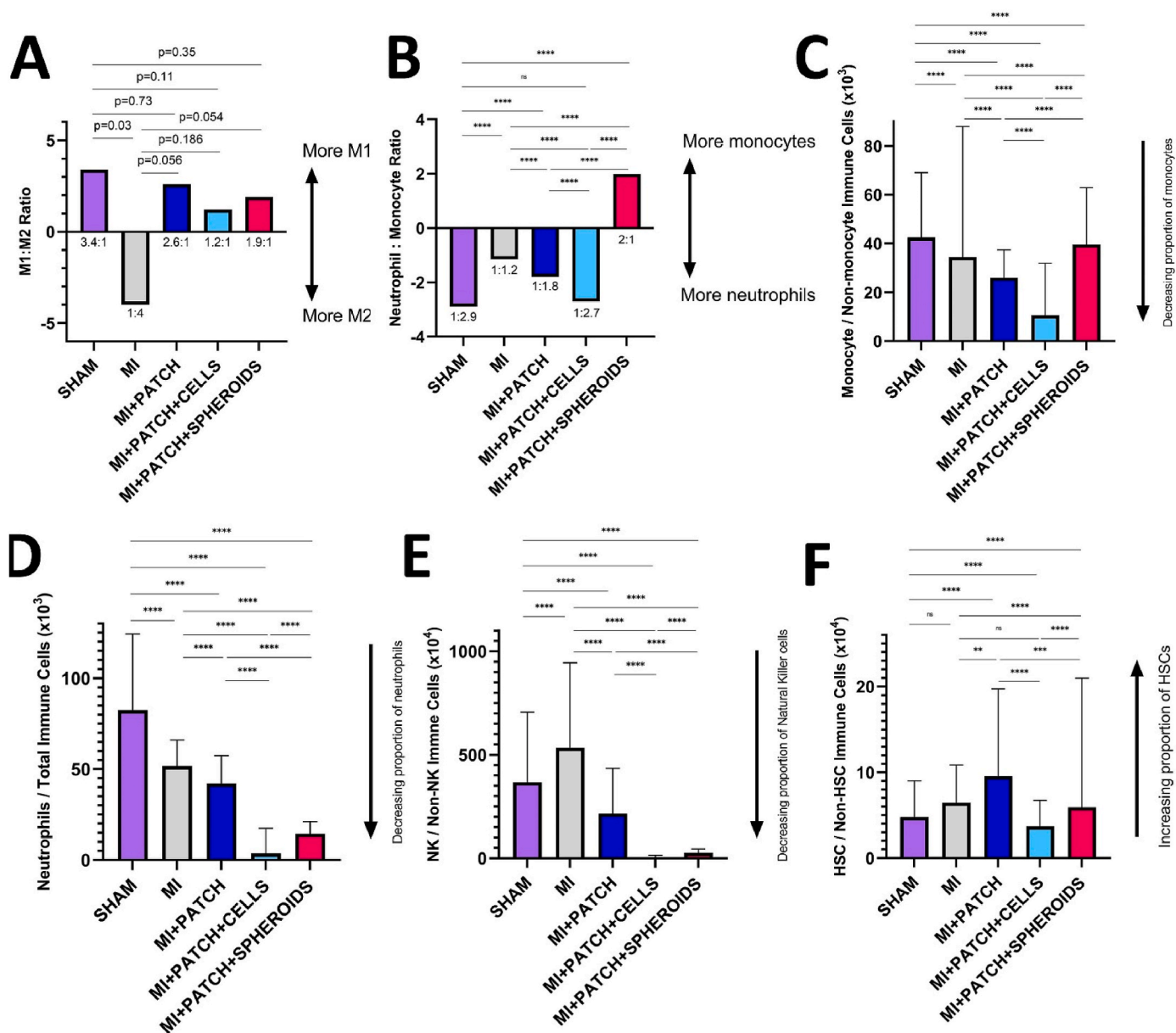
Fig. 6. Immune cell analysis at 28 days post-surgery suggests significant changes in inflammatory cell populations in heart tissue across experimental groups. (A) Macrophage analysis for experimental groups with M1 macrophage to M2 macrophage ratios (total sum M1 and M2 numbers for the whole experimental group were compared due to low numbers of events in individual mice in some groups. Absolute numbers for M1:M2/all immune cells in total were: 17:5/229180 [SHAM]; 1:4/43147 [MI]; 13:5/153252 [MI + PATCH]; 28:23/555858 [MI + PATCH CELLS]; 218:115/67448 [MI + PATCH SPHEROIDS]. Compared to sham, data show a trend towards a reversal of the M1:M2 ratio for MI which then trends towards a return to sham (not infarcted) values with any treatment (MI + PATCH, MI + PATCH CELLS or MI + PATCH SPHEROIDS. (B) Neutrophil:Monocyte whole group ratios show the spheroid group reversed the ratio seen in all other groups (to favour monocytes relative to neutrophils). (C–F) Proportion of monocytes (C), neutrophils (D), NK cells (E) and HSC (F) show significant changes in cell proportions on day 28 post surgery. Overall, these initial data point to immune cell changes warranting further dedicated analysis. Despite limitations of flow cytometry, the data suggest differences between groups and also that some modification of immune cell activity occurs whether epicardial patches contain no cells (MI + PATCH), freely suspended iPSC-CMs, iCFs, ECs (MI + PATCH CELLS) or the same cells suspended in hydrogel as spheroids (MI + PATCH SPHEROIDS). Bars show group total sum crude ratios (A–B), medians x10^3 (C–D) or x10^4 (E–F); error bars (C–F) show upper limit interquartile range.

failure patients receiving a bioprinted patch is critical in this field (already subject to ethical concerns about suboptimal media-hyped treatments [31–33]).

In this context, we analysed electrical maps and performed individual mouse sequential echocardiography (baseline – midpoint – endpoint) to identify progression in LVEF% changes (Fig. 2A). We found that relationships between electrical mapping results, infarct size and LVEF% were not straightforward, with variability in these measures due to the procedure itself (as shown by high variability in our Sham group) as well as the inherent variability of these recordings – LVEF% is known

to be highly variable, depending on heart rate, preload and afterload. It is worth noting that our day 28 analyses are based on survivors (Suppl Figure 3), which introduces an attrition bias for mice with good collaterals or with smaller infarcts. The variability inherent to infarct size, CV and LVEF% is a limitation of all animal studies in the cardiac regeneration field. Future studies should factor this in when calculating numbers to adequately power studies.

To explore the role of immune cells in host cardiac tissue, we tested for the presence of different immune cell numbers using flow cytometry (Fig. 6). We demonstrated a trend towards a reversal of the ratio of so-
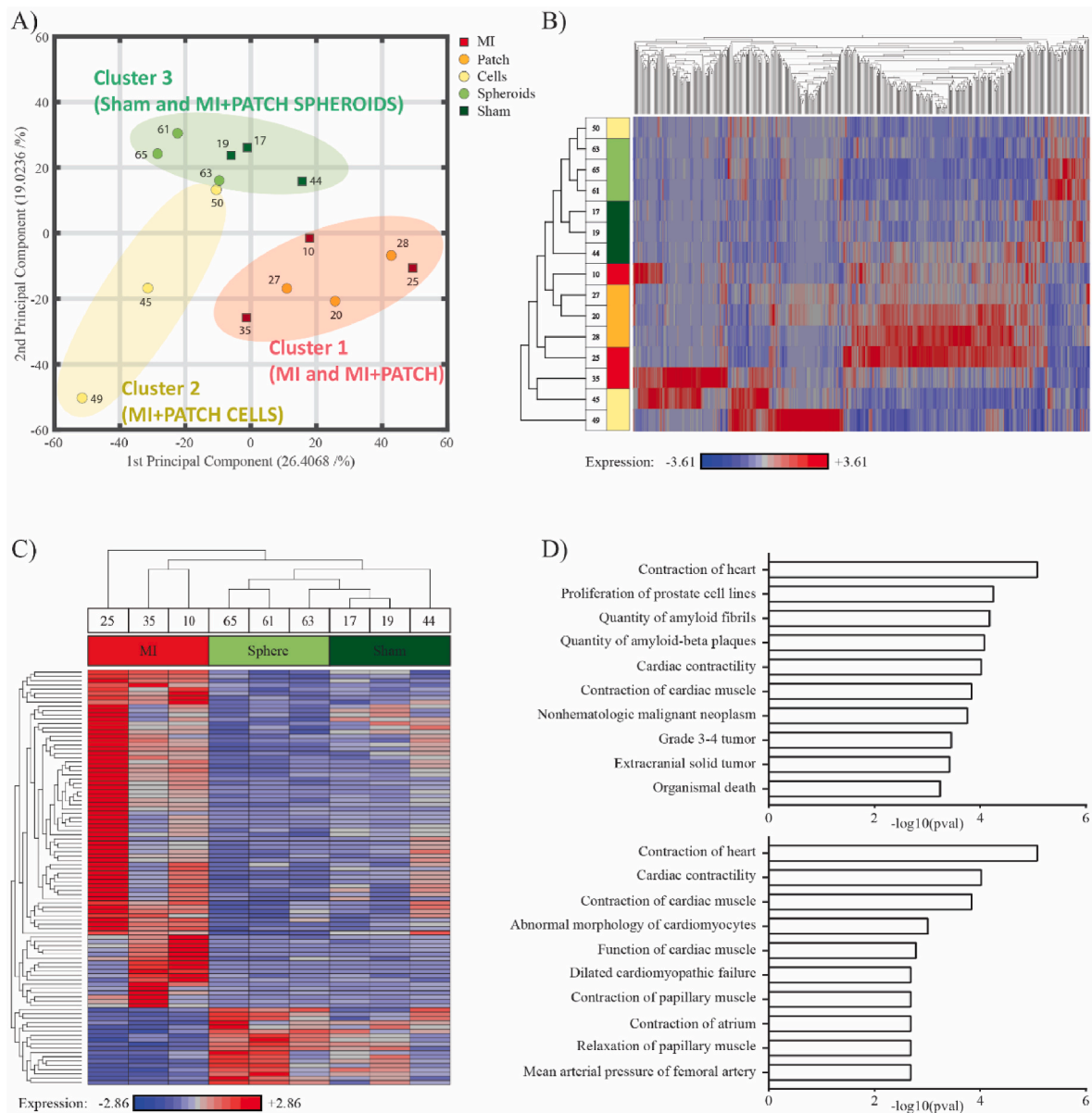
Fig. 7. The transcriptomic profile of MI + PATCH SPHEROID mice is similar to Sham mice (without MI). (A) Principal component analysis of whole transcriptome expression levels. (B) Heatmap of gene expression for all transcripts differential gene expressed between MI, Patch, Cells, Spheroids, and Sham (C) Heatmap of gene expression for all transcripts differential gene expressed between MI and Spheroids (D) Enrichment analysis for genes differentially expressed between MI and Spheroids. Diseases and Biological Functions (top panel) and Cardiovascular System Development and Functions (bottom panel).

called M1:M2 macrophages in our MI group compared to other groups (Fig. 6A). The M1:M2 ratio is a simplification, for example, it presents a complicated continuum as a dichotomy [25,34]. Nonetheless, 'classically activated' M1 macrophages have been associated with phagocytosis, elimination of tumour cells and pathogen killing, whereas 'alternatively activated' M2 macrophages have been described as profibrotic inducers of fibrosis [34]. Some have stated that M1 may exacerbate ischaemic injury whereas M2 macrophages are associated with cardioprotective effects [35], whereas others have moved away from describing macrophages in terms of M1/M2 [25,34]. Despite limitations, our findings suggest changes in macrophages with treatment groups applied after MI (all treatment groups trended towards a re-reversal of the ratio back towards an increased proportion of M1 compared to M2 macrophages). Our results might suggest that increased M1 (phagocytotic) activity compared to M2 (fibrotic) activity is important, but the results were not statistically significant due to low cell numbers in the MI group – studying depleted macrophages in the

established infarct zone is a known challenge. Our use of RAG1 mice suggests B or T cell-driven mechanisms are less important (RAG1 mice do not have mature B or T cells). Our result for NK cells (Fig. 6D) adds to the emerging evidence of the importance of these cells in MI [36]. For instance, NK cell depletion measured in our treatment groups (in particular for MI + PATCH SPHEROIDS) in consistent with improved vascular function – previous reports suggest a role played by NK cells in regulating angiotensin II-induced vascular dysfunction [37]. Other reports have also supported that reduced NK cells in MI my prevent fibrosis, [36]. This could potentially explain how reduced fibrosis observed in Fig. 4A–C could be linked to NK cell-mediated phagocytotic activity over fibrotic. Despite limitations in flow cytometry (such as batch variability), these findings complement more extensive immune cell analyses [14] and support recent understanding that innate immune system behaviour and characterisation is complex [34,38]. These data will need to be followed up with future dedicated studies, including full immunohistochemistry analysis for spatially resolved assessment of the

effects of different treatments.

Our transcriptomic analyses demonstrated that mice in the MI + PATCH SPHEROIDS group presented transcriptomic profiles similar to non-infarcted sham mice. We found that there were no differentially expressed transcripts when samples of the sham and spheroids groups were compared, suggesting that these cells were molecularly similar. RNAseq aims at broad comparison and identification of molecular avenues for detailed follow-up studies. Nonetheless, we identified interesting changes in gene expression, such as for myosin light-chain 4 (MYL4) and 7 (MYL7) which were similar for both MI vs MI + PATCH SPHEROIDS and MI vs Sham (a log2FoldChange of approximately 5, Supplementary Tables S3 and S4, respectively). Loss of MYL4 function may cause progressive atrial cardiomyopathy [39] and downregulation of MYL7 is implicated in myocardial structural abnormalities and cardiac hypertrophy [40]. For acellular (hydrogel only) compared to SPHEROID patch treatment, enrichment analyses for canonical pathways highlighted genes associated with beta adrenergic signalling and dilated cardiomyopathy (Supplementary Figs. 4–6). Further detail on cardiovascular genes and their associations is in Supplementary Tables S11 and S12. For the first time (to our knowledge), our mRNA analysis has pointed to underlying host gene expression modulation as an important potential mechanism for future studies to evaluate fully.

Our functional data (LVEF%) also showed a return to sham (non-infarcted) values for the MI + PATCH SPHEROIDS group (Fig. 2). Taken together, this supports the hypothesis that treatment with 3D bioprinted VCS patches enacted beneficial changes on underlying host gene expression. It needs to be emphasised that without splitting the VCS microtissue into its component cells and testing each as a control group, it cannot be ruled out that only one of the cell lines contained in the microtissue is contributing to these results. However, our aim was to test VCSs as a specific "microtissue" entity. We show that these can be directly suspended in AlgGel and 3D bioprinted without losing their morphological confirmation. The result was a return to the non-infarcted (sham) mRNA profile and this was not seen for other control groups.

Furthermore, VCS patch treatment enriched for genes associated with regulation of cardiac functions (contractility) and cell growth and development. The near-complete return to a transcriptomic profile resembling sham mice was not seen in the other experimental treatment groups (MI + PATCH or MI + PATCH CELLS). Along with our immune cell analysis (flow cytometry) we can therefore propose that the incremental gain in cardiac function seen between groups (patch only, freely suspended cells or cells pre-cultured as spheroids) could be due to a "dual" mechanism (gene expression as well as modulation of host inflammation). This hypothesis would require testing by a dedicated future study (beyond our descriptive/phenotypic analyses whereby it has first been proposed here). Given the high variance in our datapoints (individual mice) in the MI + PATCH CELLS group (Figs. 2B and 4D) confounding factors are possible for that group (such as patch non-adherence to the heart, missing a regional infarction on sampling or small infarct generation at LAD ligation). However, our electrical mapping data supported that the spheroid group had a favourable electrical profile (Fig. 5 and Suppl Figure 1), which is also consistent with the genetic changes we report in the spheroid group (Fig. 7).

Limitations of this study include: that patches were transplanted to the heart immediately after LAD ligation, whereas for human patients the treatment need is for chronic heart failure to restore myocardial function. Whilst many studies run up to 28 days, some have reported functional outcomes which only emerge later (8 weeks or more) [6]. Our study in mice is also not directly translatable to human trials without a large animal trial which would more closely resemble human surgery. In our model, it is also possible that difficult-to-quantify variables may have influenced outcomes, such as the extent to which a patch successfully attached and interacted with the host heart tissue underneath. We also did not analyse all immune cells, and other cell types such as mast cells may have important roles to play [41]. Systems such as the

nervous [42] and lymphatic system [43] may also be important and this is the focus of other studies [44].

Overall, our results hint at the mechanistic complexities underlying patch-based myocardial repair. A primary future direction for this study is a detailed mechanistic investigation: a dedicated study should examine our proposal that host immune responses and gene expression changes each account for part of the cardiac functional benefit we observed.

5. Conclusion

Extrusion 3D bioprinting permits hydrogel patch generation, even preserving microtissue cardiac spheroids directly suspended in the bioink. 3D bioprinted cardiac spheroid patches convey a significant improvement in cardiac function by epicardial transplantation in mice modelling MI. Gene expression changes observed only for the spheroid treatment group may explain why this group apparently returned the strongest functional improvement. Conversely, even 3D bioprinted hydrogel patches alone (without cells) partially improved heart function, suggesting that direct cardiac cell number replenishment may not be a mechanism by which cardiac function is improved (in epicardial patch-based myocardial regeneration strategies). Further preclinical studies are needed to examine mechanisms in full and answer the question why 3D bioprinted AlgGel-based patches for epicardial transplantation improve cardiac function.

Ethics statement

All procedures described in this experiment were approved by the University of Technology Sydney (UTS) Animal Care and Ethics Committee (project number ETH19-4338; 20/04/2017).

CRediT authorship contribution statement

CR: Conceptualization; Data acquisition; Data processing; Data curation; Formal analysis; Funding acquisition; Project administration; Visualization; Validation; Writing—original draft; Writing—review and editing. HL: Data generation for Figure 6); Data curation; Supervision; YH: Writing— review and editing; CdB: advice on mRNA data processing; Formal analysis; Visualisation; Supervision; Writing—review and editing. DB: (especially transcriptomic data) Data processing; Data curation; Formal analysis; Validation; Supervision; Writing— review and editing. MX: (especially flow cytometry data) Data acquisition; Data processing; Data curation; Visualisation; Supervision; Writing— review and editing. CG: Conceptualization; Data acquisition; Data processing; Data curation; Visualisation; Funding acquisition; Project administration; Visualization; Supervision; Writing—review and editing; All authors contributed to the article and approved the submitted version. Primary Guarantors (overall and data acquisition): CG and CR. Guarantors (specific): YL (electrical mapping data processing and visualisation); MX (flow cytometry data visualisation); DB (mRNA data visualisation).

Declaration of competing interest

The authors declare that they have no known competing financial interests or personal relationships that could have appeared to influence the work reported in this paper.

Data availability

The datasets associated with this experiment are available in the Supplementary Materials and the permanent data repository (https://doi.org/10.5281/zenodo.6198612). Raw confocal microscopy data for Figure 1 runs to >500GB and is therefore available from a specialist computer in the data visualisation suite at the i3 Institute

(Level 7, Building 4), Faculty of Science, University of Technology Sydney (UTS) (via request to CG). Data associated with electrical mapping is available via Yatong Li at MappingLab. Complete exported (PDF) flow cytometry data is in the data repository and the raw data (BD FACSDiva) is on a computer attached to the BD LSRFortessa™ flow cytometer at the Kolling Institute, Level 11, University of Sydney (via request to MX). Data associated with Figure 7 (gene expression) are available via DB.

Acknowledgements

Appendix A. Supplementary data

Supplementary data to this article can be found online at https://doi.org/10.1016/j.bprint.2023.e00263.

References

[1] C.D. Roche, R.J.L. Brereton, A.W. Ashton, C. Jackson, C. Gentile, Current challenges in three-dimensional bioprinting heart tissues for cardiac surgery, Eur. J. Cardio. Thorac. Surg. 58 (3) (2020) 500–510.

[2] L. Wang, V. Serpooshan, J. Zhang, Engineering human cardiac muscle patch constructs for prevention of post-infarction LV remodeling, Frontiers in cardiovascular medicine 8 (111) (2021).

[3] G.A. MacGowan, D.S. Crossland, A. Hasan, S. Schueler, Considerations for patients awaiting heart transplantation—insights from the UK experience, J. Thorac. Dis. 7 (3) (2015) 527–531.

[4] C.D. Roche, J.S. Dobson, S.K. Williams, M. Quante, J. Popoola, J.W.M. Chow, Malignant and noninvasive skin tumours in renal transplant recipients, Dermatol Res Pract 2014 (2014), 409058.

[5] L.H. Lund, K.K. Khush, W.S. Cherikh, S. Goldfarb, A.Y. Kucheryavaya, B.J. Levvey, B. Meiser, J.W. Rossano, D.C. Chambers, R.D. Yusen, J. Stehlik, The registry of the International Society for Heart and Lung Transplantation: thirty-fourth adult heart transplantation report-2017; focus theme: allograft ischemic time, J. Heart Lung Transplant. 36 (10) (2017) 1037–1046.

[6] H. Wang, C.D. Roche, C. Gentile, Omentum support for cardiac regeneration in ischaemic cardiomyopathy models: a systematic scoping review, Eur. J. Cardio. Thorac. Surg. 58 (6) (2020) 1118–1129.

[7] C.D. Roche, P. Sharma, A.W. Ashton, C. Jackson, M. Xue, C. Gentile, Printability, durability, contractility and vascular network formation in 3D bioprinted cardiac endothelial cells using alginate-gelatin hydrogels, Front. Bioeng. Biotechnol. 9 (2021), e636257.

[8] J.C. Chachques, J.C. Trainini, N. Lago, O.H. Masoli, J.L. Barisani, M. Cortes-Morichetti, O. Schussler, A. Carpentier, Myocardial assistance by grafting a new bioartificial upgraded myocardium (MAGNUM clinical trial): one year follow-up, Cell Transplant. 16 (9) (2007) 927–934.

[9] Y. Sawa, S. Miyagawa, T. Sakaguchi, T. Fujita, A. Matsuyama, A. Saito, T. Shimizu, T. Okano, Tissue engineered myoblast sheets improved cardiac function sufficiently to discontinue LVAS in a patient with DCM: report of a case, Surg. Today 42 (2) (2012) 181–184.

[10] Y. Sawa, Y. Yoshikawa, K. Toda, S. Fukushima, K. Yamazaki, M. Ono, Y. Sakata, N. Hagiwara, K. Kinugawa, S. Miyagawa, Safety and efficacy of autologous skeletal myoblast sheets (TCD-51073) for the treatment of severe chronic heart failure due to ischemic heart disease, Circ. J. 79 (5) (2015) 991–999.

[11] P. Menasché, V. Vanneaux, A. Hagege, A. Bel, B. Cholley, I. Cacciapuoti, A. Parouchev, N. Benhamouda, G. Tachdjian, L. Tosca, J.H. Trouvin, J. R. Fabreguettes, V. Bellamy, R. Guillemain, C. Suberbielle Boissel, E. Tartour, M. Desnos, J. Larghero, Human embryonic stem cell-derived cardiac progenitors for severe heart failure treatment: first clinical case report, Eur. Heart J. 36 (30) (2015) 2011–2017.

[12] P. Menasché, V. Vanneaux, A. Hagege, A. Bel, B. Cholley, A. Parouchev, I. Cacciapuoti, R. Al-Daccak, N. Benhamouda, H. Blons, O. Agbulut, L. Tosca, J. H. Trouvin, J.R. Fabreguettes, V. Bellamy, D. Charron, E. Tartour, G. Tachdjian, M. Desnos, J. Larghero, Transplantation of human embryonic stem cell-derived cardiovascular progenitors for severe ischemic left ventricular dysfunction, J. Am. Coll. Cardiol. 71 (4) (2018) 429–438.

[13] Y. Yoshikawa, S. Miyagawa, K. Toda, A. Saito, Y. Sakata, Y. Sawa, Myocardial regenerative therapy using a scaffold-free skeletal-muscle-derived cell sheet in patients with dilated cardiomyopathy even under a left ventricular assist device: a safety and feasibility study, Surg. Today 48 (2) (2018) 200–210.

[14] R.J. Vagnozzi, M. Maillet, M.A. Sargent, H. Khalil, A.K. Johansen, J. A. Schwanekamp, A.J. York, V. Huang, M. Nahrendorf, S. Sadayappan, J. D. Molkentin, An acute immune response underlies the benefit of cardiac stem-cell therapy, Nature 577 (2019) 405–409.

[15] C.D. Roche, C. Gentile, Transplantation of a 3D bioprinted patch in a murine model of myocardial infarction, JoVE (2020), e61675.

[16] L. Polonchuk, M. Chabria, L. Badi, J.C. Hoflack, G. Figtree, M.J. Davies, C. Gentile, Cardiac spheroids as promising in vitro models to study the human heart microenvironment, Sci. Rep. 7 (1) (2017) 7005.

[17] L. Polonchuk, L. Surija, M.H. Lee, P. Sharma, C. Liu Chung Ming, F. Richter, E. Ben-Sefer, M.A. Rad, H. Mahmodi Sheikh Sarmast, W.A. Shamery, H.A. Tran, L. Vettori, F. Haeusermann, E.C. Filipe, J. Rnjak-Kovacina, T. Cox, J. Tipper, I. Kabakova, C. Gentile, Towards engineering heart tissues from bioprinted cardiac spheroids, Biofabrication 13 (4) (2021), 045009.

[18] P. Sharma, C. Liu Chung Ming, X. Wang, L.A. Bienvenu, D. Beck, G. Figtree, A. Boyle, C. Gentile, Biofabrication of advanced in vitro 3D models to study ischaemic and doxorubicin-induced myocardial damage, Biofabrication 14 (2) (2022), 025003.

[19] J. Takagawa, Y. Zhang, M.L. Wong, R.E. Sievers, N.K. Kapasi, Y. Wang, Y. Yeghiazarians, R.J. Lee, W. Grossman, M.L. Springer, Myocardial infarct size measurement in the mouse chronic infarction model: comparison of area- and length-based approaches, J. Appl. Physiol. 102 (6) (2007) 2104–2111.

[20] M. Xue, H. Lin, H.P.H. Liang, K. McKelvey, R. Zhao, L. March, C. Jackson, Deficiency of Protease-Activated Receptor (PAR) 1 and PAR2 Exacerbates Collagen-Induced Arthritis in Mice via Differing Mechanisms, Rheumatology, Oxford), 2020.

[21] A. Dobin, C.A. Davis, F. Schlesinger, J. Drenkow, C. Zaleski, S. Jha, P. Batut, M. Chaisson, T.R. Gingeras, STAR: ultrafast universal RNA-seq aligner, Bioinformatics 29 (1) (2013) 15–21.

[22] Y. Liao, G.K. Smyth, W. Shi, featureCounts: an efficient general purpose program for assigning sequence reads to genomic features, Bioinformatics 30 (7) (2014) 923–930.

[23] M.I. Love, W. Huber, S. Anders, Moderated estimation of fold change and dispersion for RNA-seq data with DESeq2, Genome Biol. 15 (12) (2014) 550.

[24] RCoreTeam, R: a language and environment for statistical computing, R Foundation for Statistical Computing, Vienna, Austria. https://www.R-project.org/.

[25] A.J. Whitehead, A.J. Engler, Regenerative cross talk between cardiac cells and macrophages, Am. J. Physiol. Heart Circ. Physiol. 320 (6) (2021) H2211–h2221.

[26] Y. Li, H. Li, J. Pei, S. Hu, Y. Nie, Transplantation of murine neonatal cardiac macrophage improves adult cardiac repair, Cell. Mol. Immunol. 18 (2) (2021) 492–494.

[27] L. Wang, Y. Liu, G. Ye, Y. He, B. Li, Y. Guan, B. Gong, K. Mequanint, M.M.Q. Xing, X. Qiu, Injectable and conductive cardiac patches repair infarcted myocardium in rats and minipigs, Nat Biomed Eng 5 (2021) 1157–1173.

[28] L. Gao, Z.R. Gregorich, W. Zhu, S. Mattapally, Y. Oduk, X. Lou, R. Kannappan, A. V. Borovjagin, G.P. Walcott, A.E. Pollard, V.G. Fast, X. Hu, S.G. Lloyd, Y. Ge, J. Zhang, Large cardiac muscle patches engineered from human induced-pluripotent stem cell-derived cardiac cells improve recovery from myocardial infarction in swine, Circulation 137 (16) (2018) 1712–1730.

[29] S. Mattapally, W. Zhu, V.G. Fast, L. Gao, C. Worley, R. Kannappan, A.V. Borovjagin, J. Zhang, Spheroids of cardiomyocytes derived from human-induced pluripotent stem cells improve recovery from myocardial injury in mice, Am. J. Physiol. Heart Circ. Physiol. 315 (2) (2018) H327–h339.

[30] C. Roche, G. Iyer, M. Nguyen, S. Mabroora, A. Dome, K. Sakr, P, R, L, V, C. Wilson, C. Gentile, Cardiac Patch Transplantation Instruments for Robotic Minimally Invasive Cardiac Surgery: Initial Proof-Of-Concept Designs and Surgery in a Porcine Cadaver [preprint], Front Robot AI, 2021.

[31] F. Gilbert, J.N.M. Viana, C.D. O'Connell, S. Dodds, Enthusiastic portrayal of 3D bioprinting in the media: ethical side effects, Bioethics 32 (2) (2018) 94–102.

[32] F. Gilbert, C.D. O'Connell, T. Mladenovska, S. Dodds, Print me an organ? Ethical and regulatory issues emerging from 3D bioprinting in medicine, Sci. Eng. Ethics 24 (1) (2018) 73–91.

[33] G. Cossu, M. Birchall, T. Brown, P. De Coppi, E. Culme-Seymour, S. Gibbon, J. Hitchcock, C. Mason, J. Montgomery, S. Morris, F. Muntoni, D. Napier, N. Owji, A. Prasad, J. Round, P. Saprai, J. Stilgoe, A. Thrasher, J. Wilson, Lancet Commission: stem cells and regenerative medicine, Lancet 391 (10123) (2018) 883–910.

[34] P. Ruytinx, P. Proost, J. Van Damme, S. Struyf, Chemokine-induced macrophage polarization in inflammatory conditions, Front. Immunol. 9 (2018), 1930.

[35] J.C. Chachques, C. Gardin, N. Lila, L. Ferroni, V. Migonney, C. Falentin-Daudre, F. Zanotti, M. Trentini, G. Brunello, T. Rocca, V. Gasbarro, B. Zavan, Elastomeric cardiowrap scaffolds functionalized with mesenchymal stem cells-derived exosomes induce a positive modulation in the inflammatory and wound healing response of mesenchymal stem cell and macrophage, Biomedicines 9 (7) (2021).

[36] I. Kologrivova, M. Shtatolkina, T. Suslova, V. Ryabov, Cells of the Immune System in Cardiac Remodeling: Main Players in Resolution of Inflammation and Repair after Myocardial Infarction Frontiers in Immunology, vol. 12, 2021.

[37] S. Kossmann, M. Schwenk, M. Hausding, S.H. Karbach, M.I. Schmidgen, M. Brandt, M. Knorr, H. Hu, S. Kröller-Schön, T. Schönfelder, S. Grabbe, M. Oelze, A. Daiber, T. Münzel, C. Becker, P. Wenzel, Angiotensin II-induced vascular dysfunction depends on interferon-γ-driven immune cell recruitment and mutual activation of monocytes and NK-cells Arterioscler Thromb Vasc, Biol. 33 (2013) 1313–1319.

[38] S. Alvarez-Argote, C.C. O'Meara, The evolving roles of cardiac macrophages in homeostasis, regeneration, and repair, Int. J. Mol. Sci. 22 (15) (2021).

[39] W. Peng, M. Li, H. Li, K. Tang, J. Zhuang, J. Zhang, J. Xiao, H. Jiang, D. Li, Y. Yu, P. C. Sham, S. Nattel, Y. Xu, Dysfunction of myosin light-chain 4 (MYL4) leads to heritable atrial cardiomyopathy with electrical, contractile, and structural components: evidence from genetically-engineered rats, J. Am. Heart Assoc. 6 (11) (2017), e007030.

[40] J. Sun, X. Guo, P. Yu, J. Liang, Z. Mo, M. Zhang, L. Yang, X. Huang, B. Hu, J. Liu, Y. Ouyang, M. He, Vasorin deficiency leads to cardiac hypertrophy by targeting MYL7 in young mice, J. Cell Mol. Med. 26 (1) (2022) 88–98.

[41] S.A. Legere, I.D. Haidl, J.F. Légaré, J.S. Marshall, Mast cells in cardiac fibrosis: new insights suggest opportunities for intervention, Front. Immunol. 10 (MAR) (2019).

[42] R. Gong, Z. Jiang, N. Zagidullin, T. Liu, B. Cai, Regulation of cardiomyocyte fate plasticity: a key strategy for cardiac regeneration, Signal Transduct. Targeted Ther. 6 (1) (2021) 31.

[43] K. Klaourakis, J.M. Vieira, P.R. Riley, The evolving cardiac lymphatic vasculature in development, repair and regeneration, Nature reviews, Cardiology 18 (5) (2021) 368–379.

[44] M. Su, Z. Luo, J. Yu, R. Zhang, J. Wang, C. Huang, W. Li, W. Yuan, H. Zhang, G. Cai, S. Shen, Effects of fastigial nucleus electrostimulation on cardiac nerve regeneration, neurotransmitter release, and malignant arrhythmia inducibility in a post-infarction rat model, Eur. J. Neurosci. 54 (11) (2021) 8006–8019.